This is the accepted manuscript made available via CHORUS. The article has been published as:

Acoustic detection of electrostatic suppression of the Leidenfrost state

Arjang Shahriari, Preston S. Wilson, and Vaibhav Bahadur

Phys. Rev. E **98**, 013103 — Published 12 July 2018

DOI: 10.1103/PhysRevE.98.013103

Acoustic detection of electrostatic suppression of the Leidenfrost state

*Arjang Shahriari, Preston S. Wilson and Vaibhav Bahadur**

Department of Mechanical Engineering, The University of Texas at Austin, Austin, TX, 78712, USA

*Corresponding author: vb@austin.utexas.edu

Abstract

At high temperatures, a droplet can rest on a cushion of its vapor (the Leidenfrost effect). Application of an electric field across the vapor gap fundamentally eliminates the Leidenfrost state by attracting liquid towards the surface. This study uses acoustic signature tracking to study electrostatic suppression of the Leidenfrost state on solid and liquid surfaces. It is seen that the liquid-vapor instabilities that characterize suppression on solid surfaces can be detected acoustically. This can be the basis for objective measurements of the threshold voltage and frequency required for suppression. Acoustic analysis provides additional physical insights that would be challenging to obtain with other measurements. On liquid surfaces, the absence of an acoustic signal indicates a different suppression mechanism (instead of instabilities). Acoustic signature tracking can also detect various boiling patterns associated with electrostatically-assisted quenching. Overall, this work highlights the benefits of acoustics as a tool to better understand electrostatic suppression of the Leidenfrost state, and the resulting heat transfer enhancement.

Introduction

On sufficiently hot surfaces, a droplet can rest on its own vapor. This well-known phenomenon, known as the Leidenfrost effect, has been widely studied [1-8], with the goal of elevating the Leidenfrost temperature to prevent surface dryout. There is significant literature on

different aspects of the Leidenfrost effect including geometry of the droplet [9,10], droplet oscillations [11-15], self-propulsion of Leidenfrost droplets and Leidenfrost state-based drag reduction [16-19]. Recent studies show that an externally applied electric field in the vapor gap fundamentally eliminates [20-27] the Leidenfrost state by electrostatically attracting the droplet towards the surface. Both Direct Current (DC) [22-26] and Alternating Current (AC) [27] fields have been used for Leidenfrost state suppression on solid and liquid surfaces.

One limitation in such studies is the reliance on visual and optical measurements to infer the physics underlying suppression. In our earlier studies [22, 25, 27] high speed imaging was used to detect instabilities at the liquid-vapor interface, which indicate suppression. Celestini et al. [20] used interferometry in their study on electrical suppression. While such techniques do yield important insights, the measurements are subjective, and have significant uncertainty. Furthermore, these techniques cannot be used to study more complex situations, e.g. Leidenfrost state on a deformable liquid surface, where the vapor gap is not visible from the side.

This work uses acoustics to study electrostatic suppression of the Leidenfrost state. Previously, acoustic measurements have been used to characterize fundamental mechanisms underlying nucleate and film boiling like bubble generation, collapse and coalescence [28-39]. Bubble-related phenomena have an acoustic signature, which depends on the bubble size, superheat and liquid properties. Application-oriented studies have utilized acoustic signature tracking to understand boiling in a reactor core [29], quenching of metals [34, 35, 36] and pump cavitation [37, 38]. Acoustics has also been utilized to study droplet impact on surfaces [39]. Two recent studies [40, 41] used acoustics to confirm the existence of the Leidenfrost state. Absence of an acoustic signature indicated the Leidenfrost state; distinct sound signals were recorded upon loss of the Leidenfrost state when the droplet touched the surface.

This work uses acoustics to study various aspects of electrostatic suppression of the Leidenfrost state. Acoustic signal tracking enables objective measurements of the threshold voltage and frequency required for suppressing the Leidenfrost state. It also offers additional physical insights that would not have been possible with visual measurements. Along with droplet-based experiments, this study also uses acoustics to detect boiling patterns associated with electrostatically-assisted quenching.

Description of experiments and analysis procedure

Figure 1 shows a schematic of the experimental apparatus. Leidenfrost state suppression was studied on solid (aluminum wafer) and liquid (silicone oil pool) surfaces, on a hot plate. Surface temperature was measured with a thermocouple and an infrared camera. Droplets (isopropanol, acetone and methanol) were micropipetted on the surface (above Leidenfrost temperature) while in contact with a 100 μm diameter aluminum wire. This wire restricts droplet mobility and electrically biases the droplet; the substrate is electrically grounded. Suppression was visualized with a high-speed camera, as in previous studies [22, 27]. All experiments were repeated and the reported results are the average of at least 4 measurements.

The acoustic signature of the droplet was recorded (24-bit samples at 96 kHz) by a microphone (Earthworks M23), located 10 cm away from the droplet; the microphone was connected to a recorder (Roland R-26). All experiments were conducted in an anechoic chamber, which minimized reflections (down to 250 Hz) and provided a low ambient noise environment. Acoustic signals were analyzed using the software Raven (Cornell University). A high pass filter (>300 Hz) was applied to all measurements to eliminate low frequency noise from the experimental apparatus that was below the frequency range of interest.

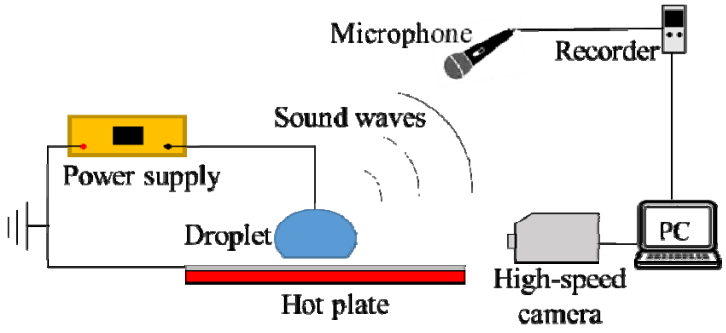

Fig. 1. Experimental apparatus for acoustic detection of electrostatic suppression of the Leidenfrost state.

Figure 2 illustrates the results and analysis methodology employed in this study. It shows the microphone signal (which is proportional to acoustic pressure) and the spectrogram (power spectrum plot of the frequency components of the sound signal versus time) associated with electrostatic suppression of the Leidenfrost state of a 30 μL isopropanol droplet on a 540 °C aluminum surface. In the absence of a voltage (left part of Figure 2), the Leidenfrost state is confirmed by the relatively low pressures of the acoustic signal (between zero and 1.5 seconds). Applying 300V (greater than threshold voltage) results in a sudden increase in the acoustic pressure, as liquid wets the surface and the Leidenfrost state is suppressed. Early stage suppression (between 1.5 and 2.5 seconds) has a higher acoustic pressure, which decreases as the droplet evaporates. After the droplet completely evaporates (4.75 seconds), the acoustic pressure returns to the original state.

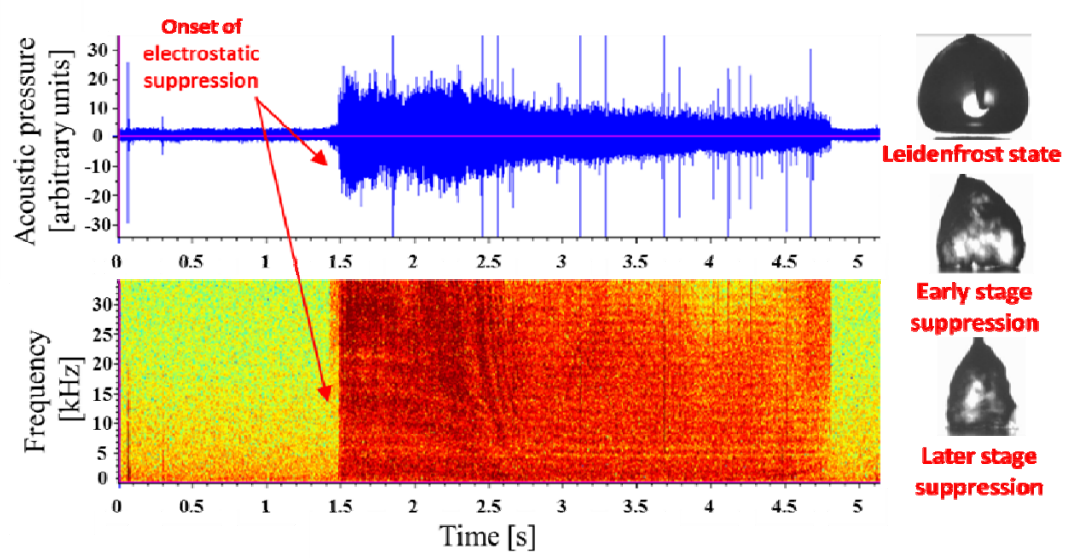

Fig. 2. Acoustic pressure and spectrogram associated with electrostatic suppression of the Leidenfrost state.

Results and discussions

Experiments were conducted to estimate the threshold DC voltage for suppression while recording the acoustic output of the process. Before delving into the results, details of the mechanism underlying suppression are briefly reviewed (they are discussed extensively in [25]). The interplay between the destabilizing force (electrostatic attraction) and stabilizing forces (capillary force and evaporation-induced pressure buildup) results in a wavy liquid-vapor interface. Above the threshold voltage, electrostatic forces dominate and the instabilities grow to bridge the vapor gap. Liquid impact on the solid surface generates an acoustic signal, which is captured by a microphone in the present work.

The microphone signal was converted to an acoustic pressure signal using a standard microphone calibrator. The RMS acoustic pressure was then calculated for the time period corresponding to suppression (e.g. between 1.5 s and 4.75 s in Fig. 2). Figure 3 shows the RMS acoustic pressure versus applied voltage for 30 μL isopropanol droplets on an aluminum

substrate at 300 °C and 540 °C. The inset of Figure 3 shows a threshold voltage of 60 V (estimated as the voltage beyond which the slope of the curve changes by 10X). In our earlier study [22], the threshold voltage was estimated by visual observation of instabilities at the liquid-vapor interface, which cause liquid fingers to bridge the vapor gap. However, visual detection is subjective and depends on the quality and magnification of imaging. In this study, such instabilities are detected visually only at 75V. The difference between the two methods is significant; these results suggest that visual measurements would over-predict the threshold voltage by 25%. It is noted that the reported RMS acoustic pressures were obtained by averaging from the onset of suppression till complete droplet evaporation. Also, the RMS acoustic pressure below threshold voltage was not zero; the ambient noise floor was 0.5 mPa.

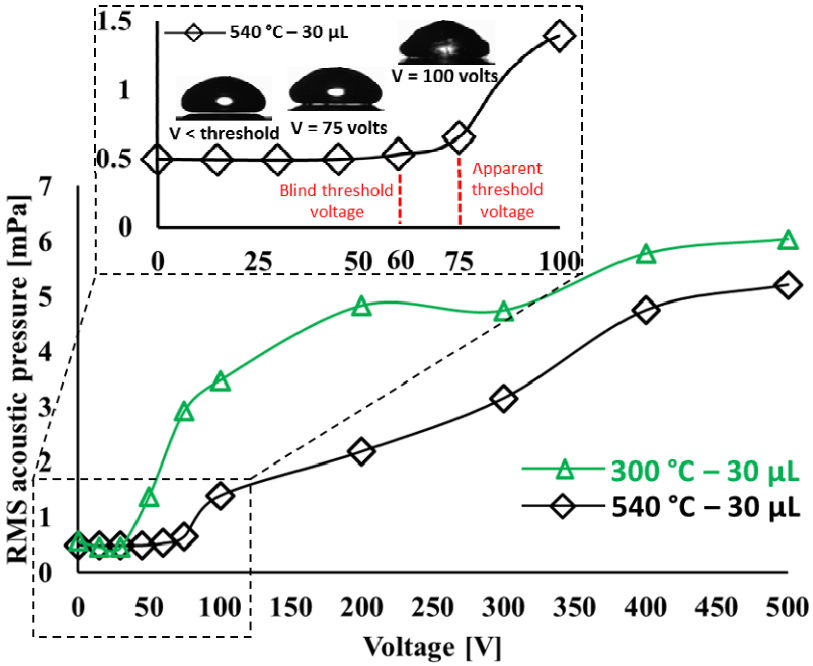

Fig. 3. RMS acoustic pressure versus applied voltage during Leidenfrost state suppression on an aluminum surface. The inset shows the threshold voltage required to initiate suppression on a 540 °C surface.

Figure 3 also shows that the RMS acoustic pressure steadily increases after the Leidenfrost state is suppressed, due to more intimate solid-liquid contact. Surface temperature influences the threshold voltage and acoustic pressures, as seen in experiments at 300 °C and 540 °C. At below-threshold voltages, the two curves overlap, due to the absence of any solid-liquid contact. Using this acoustic technique, the threshold voltage is measured to be 40V and 60V at 300 °C and 540 °C, respectively. This is expected, since a lower temperature reduces vapor pressure build-up beneath the droplet, which needs to be overcome by the electrostatic force. RMS acoustic pressure will increase in the post threshold voltage regime; however, the lower temperature surface offers less resistance to wetting, leading to more frequent instances of wetting, which elevate RMS acoustic pressures. Such distinctions are difficult to obtain from visual measurements and highlight the utility of this technique. These findings also suggest that with careful calibration, this technique can be used to estimate surface temperature.

Acoustic detection of electrostatic suppression using AC fields, was studied next. In our recent study [27], it was shown that the frequency of the AC waveform significantly determines the extent of suppression. At low frequencies (compared to the inverse of charge relaxation time), the applied electric field concentrates in the vapor gap (droplet is electrically conducting and equipotential), which maximizes the electrowetting force. As the frequency is increased, the electric field penetrates into the droplet, which reduces its strength, and therefore the extent of suppression. The threshold frequency is defined as the minimum frequency required to completely eliminate electrostatic suppression. Beyond the threshold frequency, the electric field exists in the entire droplet (which behaves as an insulator); this effectively stops suppression. The frequency of an AC waveform can thus counter the applied voltage. All these considerations are conveniently captured by the complex permittivity of the fluid [27]:

$$\varepsilon^* = \mathrm{k}\varepsilon_0 - j\frac{\sigma}{\omega} \quad (1)$$

where k is the dielectric constant, σ is the electrical conductivity and ω is the AC frequency. The first and second terms represents the capacitance and electrical resistance, respectively. As the frequency increases, the influence of electrical conductivity is reduced. Equation 1 shows that high frequencies negate the effect of the applied voltage, and eliminate suppression. The threshold frequency to eliminate suppression will also depend on the magnitude of the applied voltage.

The results of threshold frequency measurements for isopropanol droplets are shown in Figure 4 for 100 V AC and frequencies in the range 10-45 kHz. It is seen that RMS acoustic pressures decrease with increasing frequency. The threshold frequency corresponds to the plateauing of this curve and is measured to be 42.5 kHz. This is confirmed by visual absence of liquid fingering. A calculation of the charge relaxation time for isopropanol indicates a threshold frequency of 38 *kHz*, which is close to the measured value. These results again highlight the utility of acoustic techniques for objective characterization of suppression. It is noted that the ambient noise floor for AC experiments (0.9 mPa) is larger than DC experiments (0.5 mPa); this can be attributed to the acoustic noise produced by the AC function generator being louder than the DC equipment.

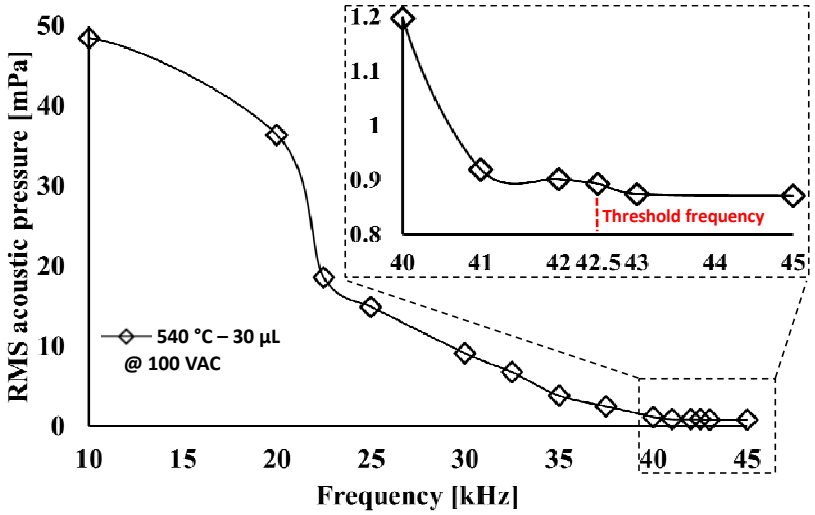

Fig. 4. AC frequency-dependent RMS acoustic pressure associated with AC electric field-induced Leidenfrost state suppression. Inset shows a zoomed-in view of data between 40-45 kHz.

Insights obtained from acoustic measurements of Leidenfrost state suppression on liquid substrates are described next. In a recent study [26], we highlighted several interesting aspects of suppression on heated silicone oil surfaces. Firstly, the Leidenfrost droplet deforms the substrate, (Figure 5a). Secondly, the electric field is distributed in the vapor gap and the silicone oil substrate. This fundamental difference in the electric field distribution (compared to conducting substrates) implies that the droplet sees a downward electrostatic force even after completely penetrating the substrate liquid. Indeed, the droplet completely sinks into the silicone oil substrate (Figure 5a). Interestingly, the threshold voltages are significantly lower [26] on silicone oil, and range from 10-25 V, depending on the thickness of the silicone oil pool. In a recent study [42], we establish that temperature gradients on the droplet and substrate surfaces enable Marangoni flow, which enhances vapor drainage in the vapor layer to significantly reduce the

vapor layer thickness. The reduction in the vapor layer thickness partly accounts for the lower voltages to suppress the Leidenfrost state on liquid substrates.

The voltage difference across the vapor gap is even lower, since a majority of the applied voltage is expressed across the silicone oil layer. These differences suggest that a different mechanism is responsible for suppression, instead of interfacial instabilities, which explain suppression on solid surfaces. Also, direct visualization of instabilities in the vapor gap is not possible, due to the deformation of the substrate.

Acoustic signature tracking conveniently overcomes this limitation. Figure 5b shows the RMS acoustic pressure versus voltage for 10 µL isopropanol droplets on silicone oil at 150 °C. No acoustic signal is detected despite suppression, which is easily confirmed visually. This clearly suggests that sound-producing instabilities and fingering events do not occur. Understanding the specific mechanism underlying suppression is beyond the scope of this study. These experiments again show the value of acoustic detection, as the absence of instabilities would have been challenging to detect using other techniques.

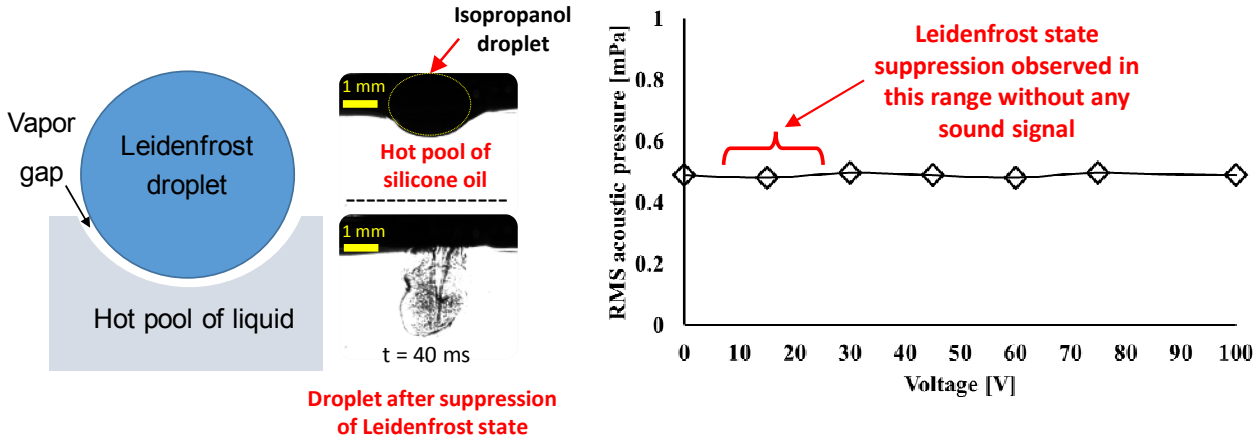

(a) **(b)**

Fig. 5. (a) Electrostatic suppression on a deformable liquid substrate [26], and (b) RMS acoustic pressure versus voltage.

The present measurements can not only pinpoint the threshold voltage, but also yield more accurate estimates of heat transfer benefits of suppression. To first order, the heat dissipation capacity can be estimated by measuring the droplet evaporation rate (image processing). The heat dissipation capacity can be predicted using $q''=(m.h_{fg})/(A.t_b)$, where m is droplet mass, h_{fg} is latent heat of vaporization, t_b is the droplet lifetime and A is the solid-liquid contact area. Our previous estimate [22] was based on the footprint area of the droplet on the surface; however, this is inaccurate since the droplet does not wet 100% of the footprint area. The actual liquid-solid contact area can be estimated by linearly scaling the area in proportion to the measured RMS acoustic pressure at a particular voltage. This hypothesis assumes that the number of solid-liquid contact events influence the contact area and the generated acoustic pressure in the same manner. Acoustic measurements also enable more accurate measurements of the droplet lifetime.

Figure 6 compares the presently-estimated heat dissipation capacity with previous estimates [22]. It is seen that the heat dissipation capacity, when factoring in the actual solid-liquid contact area (under the hypothesis that the contact area scales linearly with the acoustic pressure), is significantly higher than the apparent heat dissipation capacity. The actual heat dissipation capacity is up to 270% higher than previously estimated. This study reports heat flux dissipation exceeding 400 W/cm^2 for evaporating droplets. This exercise again highlights the utility of acoustics as a tool for better understanding the thermo-fluidics of the Leidenfrost state.

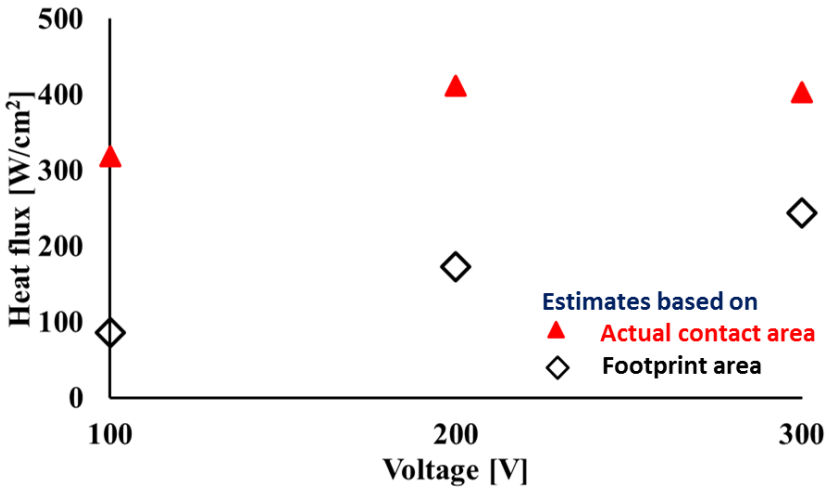

Fig. 6. Estimated heat dissipation capacity associated with droplets where the Leidenfrost state is electrostatically suppressed.

The final set of experiments were about electrostatically-assisted quenching of metals. At very high temperatures, typical of quenching, a vapor film forms on the surface. This film can be electrostatically suppressed [23], which significantly accelerates the cooling rate. In this study, heated 2.54-cm-diameter copper spheres were immersed in an isopropanol bath. The sphere had an ungrounded K-type thermocouple at the center. A wire biased the sphere and a potential difference across the vapor gap was established by a grounded electrode in the bath. The apparatus and procedure previously described were employed again, but the microphone was replaced with a hydrophone (Teledyne Reson TC4013) submerged in the liquid bath, 5 cm away from the sphere. The acoustic signature of the quenching process was recorded and hydrophone signals were converted into acoustic pressure signatures using factory calibration.

Images of the sphere in Figure 7 show various boiling stages during cooldown. Film boiling is immediately suppressed by the applied electric field; the resulting pattern can be termed as transition boiling, with any point on the surface alternating contacting vapor and liquid. At lower temperatures, the pattern changes to nucleate boiling (characterized by discrete bubbles),

followed by natural convection. Figure 7 also shows the temperature-time curve and the RMS acoustic pressure-time curve in the absence and presence of an electric field. The fundamental switch from film boiling (no voltage) to transition boiling (applied voltage) in the initial phase drastically alters the cooling curve.

The RMS acoustic pressure curve in Figure 7 yields several important insights. Firstly, acoustic measurements clearly detect transitions to nucleate boiling (from film and transition boiling). Prior to these transitions, RMS acoustic pressures are larger for the electrowetted case (~ 3.2 Pa) compared to the non-electrowetted case (~ 2.6 Pa). Secondly, when the temperatures reach ~ 150 °C, the switch to nucleate boiling and resulting collapse of the vapor gap generates much higher acoustic pressures. The peak RMS acoustic pressure for the electrowetted case (66 Pa) is smaller than the non-electrowetted case (86 Pa), likely due to the smaller vapor gap resulting from the applied voltage. In the nucleate boiling region, the RMS acoustic pressures are 5.3 Pa and 4.1 Pa for the non-electrowetted and electrowetted cases, respectively. These amplitudes depend on various bubble-related phenomena, which also depend on the electric field. Finally, the acoustic signature of the natural convection region is almost identical for the two cases. This is expected since the influence of the electric field is no longer at play (due to the absence of the vapor gap). Together, all these results highlight the wealth of information that can be inferred from acoustic signature tracking of electrostatically-assisted quenching.

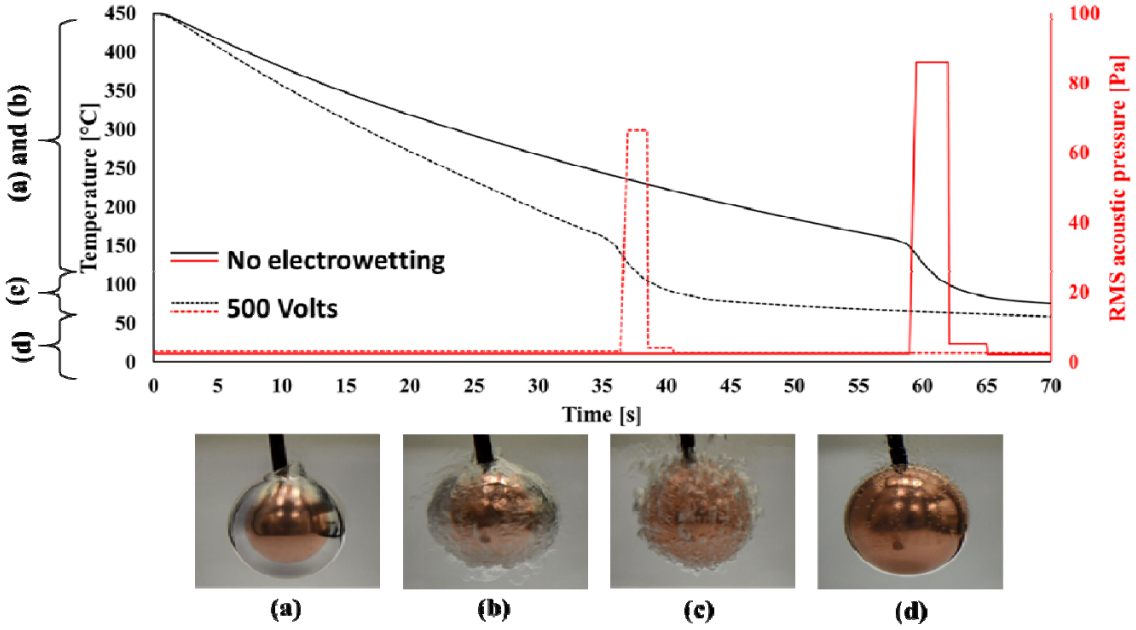

Fig. 7. Acoustic signature tracking of electrostatically-assisted quenching. Temperature and RMS acoustic pressure variation is shown along with various boiling patterns observed during cooldown: (a) Film boiling, (b) Transition boiling, (c) Nucleate boiling and (d) Natural convection.

In conclusion, this study shows acoustics as a powerful tool to analyze electrically enhanced boiling in droplet and pool boiling configurations. Threshold voltage/frequency and the transition between various boiling regimes can be objectively determined by tracking the acoustic signature. With appropriate calibration, this technique can also be used to estimate surface temperatures, heat flux and onset of dryout associated with electrically enhanced boiling.

Acknowledgements

The authors acknowledge National Science Foundation grant no. CBET-1605789 for supporting this work. Assistance of Onur Ozkan for conducting quenching experiments is also acknowledged.

References

1. Roh, H. Heat transfer mechanisms in pool boiling. *Int. J. Heat Transf.* **68,** 332–342 (2012).
2. Biance, A-L., Clanet, C., Quere, D. Leidenfrost drops. Phys. Fluids, **15**, 1632-1637 (2003).
3. Kwon, H. M., C., B. J., Varanasi, K. K. Increasing Leidenfrost point using micro-nano hierarchical surface structures. *Appl. Phys. Lett.* **103,** 201601 (2013).
4. Vakarelski, I. U., Patankar, N. A., Martson, J. O., Chan, D. Y. C., Thoroddsen, S. T. Stabilization of Leidenfrost vapour layer by textured superhydrophobic surfaces. *Nature* **489,** 274–277 (2012).
5. Chu, K.-H., Enright, R., Wang, E. N. Structured surfaces for enhanced pool boiling heat transfer. *Appl. Phys. Lett.* **100,** 241603 (2012).
6. Maquet, L., Sobac, B., Darbois-Texier, B., Duchesne, A., Brandenbourger, M., Rednikov, A., Colinet, P., Dorbolo, S. Leidenfrost drops on a heated liquid pool. Phys. Rev. Fluids, **1**, 053902 (2016).
7. Sajadi, S. M., Irajizad, P., Kashyap, N., Farokhnia, N., Ghasemi, H. Surfaces for high heat dissipation with no Leidenfrost limit. *Appl. Phys. Lett.* **100,** 241603 (2012).
8. Farokhnia, N., Sajadi, S. M., Irajizad, P., Ghasemi, H. Decoupled Hierarchical Structures for Suppression of Leidenfrost Phenomenon. *Langmuir*, **33**, 2541-2550 (2017).
9. Snoeijer, J.H., Brunet, P. and Eggers, J. Maximum size of drops levitated by an air cushion. *Physical Review E*, **79(3)**, p.036307 (2009).
10. Burton, J.C., Sharpe, A.L., Van Der Veen, R.C.A., Franco, A., Nagel, S.R. Geometry of the vapor layer under a Leidenfrost drop. *Physical Review Letters*, **109(7)**, p.074301

(2012).

11. Bouwhuis, W., Winkels, K.G., Peters, I.R., Brunet, P., Van Der Meer, D., Snoeijer, J.H. Oscillating and star-shaped drops levitated by an airflow. *Physical Review E*, **88(2)**, p.023017 (2013).

12. Caswell, T.A. Dynamics of the vapor layer below a Leidenfrost drop. *Physical Review E*, **90(1)**, p.013014 (2014).

13. Ma, X., Liétor-Santos, J.J., Burton, J.C. The many faces of a Leidenfrost drop. *Physics of Fluids*, **27(9)**, p.091109 (2015).

14. Ma, X., Liétor-Santos, J.J., Burton, J.C. Star-shaped oscillations of Leidenfrost drops. *Physical Review Fluids*, **2(3)**, p.031602 (2017).

15. Ma, X., Burton, J.C. Self-organized oscillations of Leidenfrost drops. *Journal of Fluid Mechanics*, **846**, pp.263-291 (2018).

16. Linke, H., Alemán, B.J., Melling, L.D., Taormina, M.J., Francis, M.J., Dow-Hygelund, C.C., Narayanan, V., Taylor, R.P., Stout, A. Self-propelled Leidenfrost droplets. *Physical Review Letters*, **96(15)**, p.154502 (2006).

17. Lagubeau, G., Le Merrer, M., Clanet, C., Quéré, D. Leidenfrost on a ratchet. *Nature Physics*, **7(5)**, p.395 (2011).

18. Vakarelski, I.U., Marston, J.O., Chan, D.Y., Thoroddsen, S.T. Drag reduction by Leidenfrost vapor layers. *Physical Review Letters*, **106(21)**, p.214501 (2011).

19. Vakarelski, I.U., Chan, D.Y. and Thoroddsen, S.T. Leidenfrost vapour layer moderation of the drag crisis and trajectories of superhydrophobic and hydrophilic spheres falling in water. *Soft Matter*, **10(31)**, pp.5662-5668 (2014).

20. Celestini, F., Kirstetter, G. Effect of an electric field on a Leidenfrost droplet. *Soft Matter*

8, 5992 (2012).

21. Sur, A., Lu, Y., Pascente, C., Ruchhoeft, P., Liu, D. Pool booiling heat transfer enhancement with electrowetting. *Int. J. Heat Mass Transfer*, **120**, 202-217 (2018).
22. Shahriari, A., Wurz, J., Bahadur, V. Heat transfer enhancement accompanying Leidenfrost state suppression at ultrahigh temperatures. *Langmuir* **30,** 12074–81 (2014).
23. Shahriari, A., Hermes, M., Bahadur, V. Electrical control and enhancement of boiling heat transfer during quenching. *Appl. Phys. Lett.* **108,** (2016).
24. Shahriari, A., Birbarah, P., Oh, J., Miljkovic, N., Bahadur, V. Electric-field-based control and enhancement of boiling and condensation. *Nanoscale Microscale Thermophys. Eng.,* **21**, 102-121 (2016).
25. Shahriari, A., Das, S., Bahadur, V., Bonnecaze, R. T. Analysis of the instability underlying electrostatic suppression of the Leidenfrost state. *Phys. Rev. Fluids* **2,** (2017).
26. Shahriari, A., Ozkan, O., Bahadur, V. Electrostatic suppression of the Leidenfrost state on liquid substrates. *Langmuir*, **33** , 13207–13213 (2017).
27. Ozkan, O., Shahriari, A., Bahadur, V. Electrostatic suppression of the Leidenfrost state using AC electric fields. *Appl. Phys. Lett.*, **111**, 141608 (2017)
28. Lykof, E.V., Sinetskaya, A.G. Transient process and thermoacoustic effects in surface boiling of a liquid. *Journal of Engineering Physics and Thermophysics*, **78**, 646-650 (2005).
29. Kwatny, H.G., Fink, L.H. Acoustics, stability, and compensation in boiling water reactor pressure control systems. *IEEE transactions on automatic control*, 20, 727-739, (1975).
30. Carmi, R., Bussiba, A., Widenfeld, G., Aharon, Y., Alon, I., Hochbaum, I. Detection of transient zones during water boiling by acoustic emission. *J. Acoustic Emission*, **29**, 89-97

(2011).

31. Korolev, A.V., Litvin, A.N. Investigation of noises in boiling on an electrically heated wire. *Journal of Engineering Physics and Thermophysics,* **75**, 1033-1036 (2002).

32. Smrke, A., Prezlej, J., Steblaj, P., Smrke, I. Sound of boiling as a disturbing noise and as a functional signal. MIPRO (2012).

33. Alhashan, T., Elforjani, M., Addali, A., Teixeira, J. Monitoring of Bubble Formation during the Boiling Process Using Acoustic Emission Signals. *Int. J. Eng. Res. Sci*, **2**, 66-72 (2016).

34. Ravnik, F. Grum, J. Heat Transfer Stages Recognition by Boiling Acoustic During Quenching. *Film and Nucleate Boiling Processes. ASTM* International (2012).

35. Ravnik, F., Grum, J. Relation between sound emission occurring during quenching and mechanical properties of the steel after quenching. *BHM Berg-und Hüttenmännische Monatshefte*, **155**, 119-124 (2010).

36. Mojškerc, B., Kek, T., Grum, J. Feasibility study of monitoring the steel quenching process using acoustic emission technology. *Applied Acoustics*, **129**, 335-345 (2018).

37. Neil, G.D., Reuben, R.L., Sandford, P.M., Brown, E.R., Steel, J.A. Detection of incipient cavitation in pumps using acoustic emission. *Proceedings of the Institution of Mechanical Engineers, Part E: Journal of process mechanical engineering*, 211, 267-277 (1997).

38. Cudina, M. Detection of cavitation phenomenon in a centrifugal pump using audible sound. *Mechanical systems and signal processing*, 17, 1335-1347 (2003).

39. Oguz, H.N., Prosperetti, A. Bubble entrainment by the impact of drops on liquid surfaces. *Journal of Fluid Mechanics*, 219, 143-179 (1990).

40. Grounds, A., Still, R., Takashina K. Enhanced droplet control by transition boiling.

Scientific Reports, **2**, 720 (2012).

41. Padilla, J., Carey V.P. Water droplet vaporization on superhydrophilic nanostructured surfaces at high and low superheat. *Proceedings of the ASME 2014 International Mechanical Engineering Congress and Exposition IMECE* (2014).

42. Shahriari, A., Acharya, P., Bahadur, V. Modeling the influence of Marangoni flows on the Leidenfrost state on solid and liquid substrates. Proceedings of the 16th International Conference on Nanochannels, Microchannels and Minichannels (ICNMM) (2018), Dubrovnik, Croatia.